A&A 595, A31 (2016)
DOI: 10.1051/0004-6361/201526404

Astronomy & Astrophysics

Sparse aperture masking at the VLT

II. Detection limits for the eight debris disks stars β Pic, AU Mic, 49 Cet, η Tel, Fomalhaut, g Lup, HD 181327 and HR 8799[⋆,⋆⋆]

L. Gauchet[1], S. Lacour[1], A.-M. Lagrange[2,3], D. Ehrenreich[4], M. Bonnefoy[2,3], J. H. Girard[5], and A. Boccaletti[1]

[1] LESIA, Observatoire de Paris, PSL Research University, CNRS, Sorbonne Universités, Univ. Paris Diderot, UPMC Univ. Paris 06, Sorbonne Paris Cité, 5 place Jules Janssen, 92195 Meudon, France
e-mail: lucien.gauchet@obspm.fr
[2] Univ. Grenoble Alpes, IPAG, 38000 Grenoble, France
[3] CNRS, IPAG, 38000 Grenoble, France
[4] Observatoire de l'Université de Genève, 51 chemin des Maillettes, 1290 Sauverny, Switzerland
[5] European Southern Observatory, Casilla 19001, Santiago 19, Chile

Received 24 April 2015 / Accepted 2 June 2016

ABSTRACT

Context. The formation of planetary systems is a common, yet complex mechanism. Numerous stars have been identified to possess a debris disk, a proto-planetary disk or a planetary system. The understanding of such formation process requires the study of debris disks. These targets are substantial and particularly suitable for optical and infrared observations. Sparse aperture masking (SAM) is a high angular resolution technique strongly contributing to probing the region from 30 to 200 mas around the stars. This area is usually unreachable with classical imaging, and the technique also remains highly competitive compared to vortex coronagraphy.
Aims. We aim to study debris disks with aperture masking to probe the close environment of the stars. Our goal is either to find low-mass companions, or to set detection limits.
Methods. We observed eight stars presenting debris disks (β Pictoris, AU Microscopii, 49 Ceti, η Telescopii, Fomalhaut, g Lupi, HD 181327, and HR 8799) with SAM technique on the NaCo instrument at the Very Large Telescope (VLT).
Results. No close companions were detected using closure phase information under 0.5″ of separation from the parent stars. We obtained magnitude detection limits that we converted to Jupiter masses detection limits using theoretical isochrones from evolutionary models.
Conclusions. We derived upper mass limits on the presence of companions in the area of a few times the telescope's diffraction limits around each target star.

Key words. instrumentation: high angular resolution – planetary systems – planets and satellites: formation

1. Introduction

Disk evolution is a key question in the comprehension of planetary system formation as they are intrinsically linked together. Thus direct detection and imaging of planets in such disks are mandatory to understand how planetary systems form and evolve. A debris disk is composed of dust grains and small bodies orbiting around the star, it is usually gas-poor, and grain sizes are typically one to hundred of micrometers. The debris disks depletion process is recognized to be short (~10 Myr or less) but many disks have been found to last longer. The presence of large planetary bodies can induce sufficient gravitational perturbations to provoke collisions of planetesimals, the result is smaller fragments that replenish the circumstellar environment. Thus debris disks may be good indicators of planetary systems or ongoing planet formation.

The disks can be observed thanks to scattered light and thermal emission of the dust grains. Identification of infrared (IR) excess in the spectral energy distribution led to the first extrasolar debris disk detection around Vega (Aumann et al. 1984).

β Pictoris is a remarkable system because of its young age estimated between 8 and 20 Myr (Zuckerman et al. 2001). The existence of a planet (Lagrange et al. 2010) orbiting around β pictoris makes it a benchmark for testing planetary formation models. Several scenarios were formalized, such as accretion, gravitational instabilities, or a combination of both (Bonnefoy et al. 2013). It is important to understand which processes are involved in such formation and estimate to what extent they contribute to it. Other young planets exist (e.g. HR 8799). It is thus absolutely important to find other planets or debris disks stars to multiply reference points.

This paper aims to study eight objects around which debris disks have already been discovered. It is necessary to investigate the close environment of the star that is usually inaccessible to imaging techniques like coronagraphy and point spread function (PSF) subtraction algorithms (ADI, LOCI, PCA, etc.). Sparse aperture masking (SAM) has a small inner working angle, and has a unique ability to probe the region between $\frac{\lambda}{2D}$ and $\frac{2\lambda}{D}$, with

⋆ Based on observations collected at the European Southern Observatory (ESO) during runs 087.C-0450(A), 087.C-0450(B) 087.C-0750(A), 088.C-0358(A).
⋆⋆ All magnitude detection limits maps are only available at the CDS via anonymous ftp to cdsarc.u-strasbg.fr (130.79.128.5) or via http://cdsarc.u-strasbg.fr/viz-bin/qcat?J/A+A/595/A31

Table 1. Log of SAM observations with VLT/NACO.

Star	UT date y/m/d	Mask	DIT (s)	NDIT	NEXP	Seeing[1]	τ_0[2] (ms)	Calibrator
g Lup	2011/06/08	7 holes	0.08	500	40	0.76	3.2	HD 139960
49 Cet	2011/08/04	7 holes	0.08	500	40	0.67	1.5	HD 10100
Fomalhaut	2011/08/04	BB 9 holes	0.02	2000	32	0.68	2.1	del PsA
HD 181327	2011/08/04	7 holes	0.106	472	40	0.80	2.3	HD 180987
HR 8799	2011/08/04	7 holes	0.051	785	40	0.77	1.6	HD 218234
AU Mic	2011/08/31	7 holes	0.04	600	104	0.82	3.1	HD 197339
η Tel	2011/09/01	7 holes	0.01	500	56	0.96	2.1	HD 181517
β Pic	2011/10/12	7 holes	0.04	800	64	1.8	0.6	HR 2049

Notes. (1) Provided using keyword `TEL IA FWHM`; (2) provided using keyword `TEL AMBI TAU0`.

high-contrast capabilities (with a dynamic of a few thousands). It includes the area from 30 to 200 mas, which is equivalent to a distance of 1.5 to 10 AU for a star located at 50 pc, as for β Pic, η Tel, HR 8799 and AU Mic. These separations correspond to regions in primordial disks where planets can efficiently form by core accretion Kennedy & Kenyon (2008).

In Sect. 2 we describe aperture masking observations performed on NaCo at the Very Large Telescope (VLT) and the data reduction technique, in Sect. 3 we report our observational results in terms of mass limits of companions for each systems. In Sect. 4 we present our conclusions.

2. Observations and data reduction

2.1. Observations

The eight systems imaged, among which β Pictoris and HR 8799, are listed in Table 1. They were observed at the VLT from June to October 2011 using NAOS-CONICA (NaCo) providing adaptive optics assisted imaging.

We used the sparse aperture mode to achieve the highest angular resolution at the diffraction limit. This technique described in Tuthill et al. (2000) uses a mask with holes in non-redundant configuration placed in a pupil plane of the instrument. The goal of this mask is to transform the main pupil of the telescope into an interferometric array. Each baseline made of any pair of sub-apertures will create a fringe pattern that is unique in terms of direction and spatial frequency. This allows us to overcome the non-coherent addition of the wavefront in the focal plane.

The observations were carried out in the L'-band (λ_c = 3.80 μm, $\Delta\lambda$ = 0.62 μm) using two of the four masks available on NaCo, the broadband (BB) nine holes, and the seven holes masks. Observational details such as mask used, integration time (DIT), size of datacube, and number of exposures for each science target are summarized in Table 1.

The operational mode for observation was to image the star with the masked pupil in each of the four quadrants of the L27 camera of NaCo (the four 128 × 128 pixels quadrants from the 256 × 256 pixels detector). An example of PSF and respective power spectrum obtained with Fomalhaut are displayed in Fig. 1. Each target is alternately observed with a calibrator star. This provides a PSF reference in order to calibrate the science data. This process benefits from the SAM "star hopping" strategy allowing a fast switch between science star and calibrator. As long as the two targets have comparable brightness on the wavefront sensor it is possible to jump from one to the other without requiring a full optimization of the adaptive optic (AO) loop and its associated time penalty. Thus we get very similar atmospheric perturbation over both science and respective calibrator's data. This significantly improves accuracy on calibration and results in higher performance over detection limits.

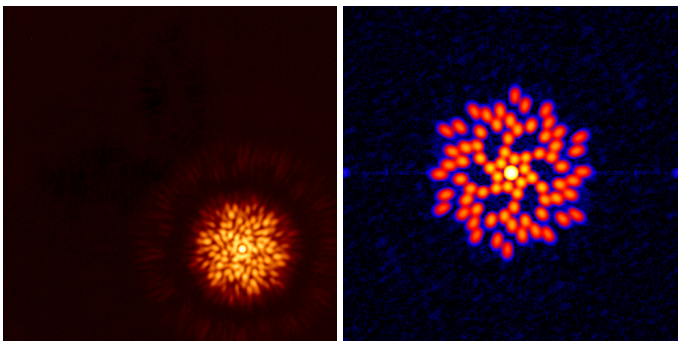

Fig. 1. *Left*: image of Fomalhaut on the 256 × 256-pixel CONICA detector. The detector field-of-view is 7″; i.e., each pixel is 27 mas in size on sky. The ~2.6 arcsec point spread function is due to diffraction of the 78 cm holes in the 9-holes mask used during this observation. The many speckles apparent inside this large Airy pattern are due to the superposition of fringes caused by the 36 spatial frequencies allowed through the mask. *Right*: power spectrum i.e. squared amplitude of Fourier's components from the Fomalhaut PSF in the spatial frequency domain.

2.2. SAM pipeline

The data was reduced using the sparse aperture mode pipeline (SAMP) written in the Yorick interpreted language. Description and operating details of the pipeline are available in Lacour et al. (2011). Here we summarize the main method of reduction. In the first stage, data is corrected from systematic alterations: images are flat-fielded, bad-pixels removed, sky-subtracted. This step is particularly important as the sky luminosity is dominant in L'-band. Quadrant images from the eight-point offset pattern are aligned, centered and stacked. Direct fringes fitting is then performed to get complex visibilities from the fringes (see Greenbaum et al. 2015). Amplitude and phase of the fringes are strongly affected by the atmospheric turbulence. To overcome perturbations from the atmosphere, we use the closure phase quantity (e.g. Baldwin et al. 1986; Haniff et al. 1987) which takes into account the symmetry of the object. It consists in the linear combination of phases over a triangle of baselines. This quantity has the interesting property of being independent from the atmospheric piston. More precisely, complex visibilities are multiplied together to form the triple product called bispectrum. Closure phases are obtained from the argument of the bispectrum

Table 2. List of stars used in this work, provided with specifications: distance from the observer, estimated age and spectral type of the parent star.

Object	Distance (pc)	Age (Myr)	Spectral type	K^1 (mag)	L'^2 (mag)	References
49 Cet	59	40	A1V	5.46	5.45	1, 2
AU Mic	9.9	$21^{\pm4}$	M1Ve	4.53	4.32	3, 4, 5
β Pic	19.3	$21^{\pm4}$	A6V	3.48	3.46	5, 6
η Tel	47.7	$21^{\pm4}$	A0V	5.01	5.01	1, 5, 7
Fomalhaut	7.7	$440^{\pm40}$	A3V/A4V	1.05	1.04	6, 8
g Lup	17.5	300^{+700}_{-200}	F5V	3.80	3.76	1, 9, 10
HD 181327	51.8	$21^{\pm4}$	F5V/F6V	5.91	5.87	1, 5, 11, 12
HR 8799	39.4	30^{+20}_{-10}	F0V	5.24	5.22	2, 13

Notes. (1) Provided by SIMBAD database; (2) derived with Tokunaga (2000) color table.

References. (1) Cutri et al. (2003); (2) van Leeuwen (2007); (3) Stauffer et al. (2010); (4) Torres et al. (2006); (5) Binks & Jeffries (2014); (6) Ducati (2002); (7) Wyatt et al. (2007); (8) Mamajek (2012); (9) Gray et al. (2006); (10) Kalas et al. (2006); (11) Schneider et al. (2006); (12) Holmberg et al. (2009); (13) Gray & Corbally (2014).

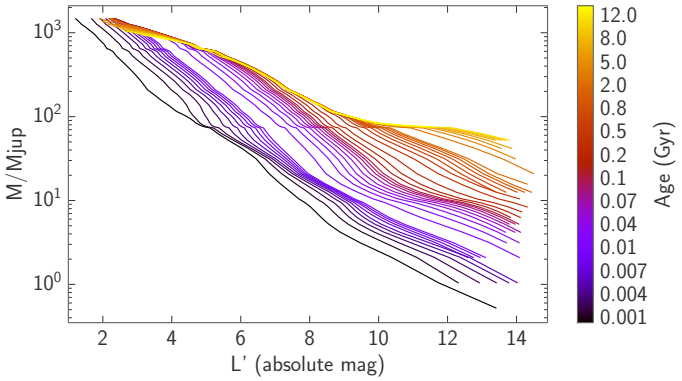

Fig. 2. Theoretical isochrones showing L' emission magnitude with mass of the object.

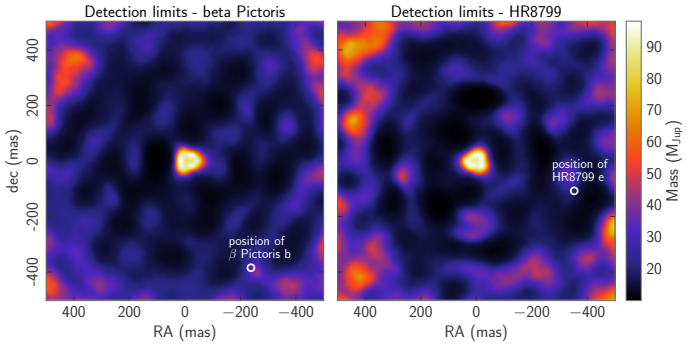

Fig. 3. Sample of detection limits maps obtained for β Pictoris (*left*) and HR 8799 (*right*).

(Weigelt 1977; Lohmann et al. 1983). All closure phases are calibrated by subtraction of the closure phases from the calibrator stars mentioned in Sect. 2.1.

The observed closure phases are then fit with a binary model with three parameters: separation δ, position angle α and luminosity ratio ρ. A cube of χ^2 values from each triplet (α, δ, ρ) is built. Since no clear detection is present in our dataset, the $\chi^2(\alpha, \delta, \rho)$ cube is scaled so that the reduced χ^2 is equal to 1 for $\rho = 0$ (no companion). Detection limits are then obtained for each α and δ as $\tilde{\rho}$ such as $\chi^2(\alpha, \delta, \tilde{\rho}) < 25 + \chi^2(0, 0, 0)$. In other words, the detection limits are calculated as the minimum value for which the χ^2 is below 5σ of a non detection.

2.3. Detection limits: from magnitude to mass

The examination of closure phases did not allow us to rule on the presence or not of a faint companion in the data sets. However, study of the χ^2 maps allows for the extraction of detection limits.

Detection limit maps from the *SAM pipeline* are expressed in contrast ratio. Hence, the L' band detection limits depend on the brightness of the parent star. We used the spectral type of the stars (given in Table 2), combined with Tokunaga (2000) tables of intrinsic colors for main sequence, giant and super giant stars, to derive the L' absolute magnitude of the stars. The magnitudes are listed in the Table 2. At this point, we obtain detection limits in terms of absolute L' magnitude[1].

To estimate the mass as a function of the luminosity, we used the theoretical isochrones established by Baraffe et al. (1997, 1998, 2003). More specifically, we used the BT-Settl model (Allard et al. 2012). Those isochrones were interpolated into synthetic color tables and converted into the VLT NaCo filters systems[2]. Other evolutionary models do exist and are based on similar or alternative planet formation scenarios, such as the "warm-start" model proposed by Spiegel & Burrows (2012). The mass/luminosity isochrones derived from other models can be perfectly applied to the data we made available at the CDS. Figure 2 displays the theoretical isochrones for L' magnitude versus the mass of the object. Given the commonly accepted age of the parent star/debris disk and the absolute magnitude of the detection limit, we derive the associated mass. Examples of two-dimensional mass detection limit maps for β Pictoris and HR 8799 are displayed in Fig. 3.

3. Results

From the two-dimension maps, we determine a radial distribution of the detection limits. It is obtained by computing the minimum and the maximum value in 5 mas thick rings. The computation was done for radii between 30 to 500 mas. This process

[1] Detection limits maps are available in electronic form at the CDS.
[2] https://phoenix.ens-lyon.fr/Grids/BT-Settl/

allows to keep the information on variations over azimuthal position at a given radius. The radial detection limits for each target are displayed in Fig. 4. Table 3 summarizes the highest contrast achieved in the 30–200 mas separation range – where SAM is the most efficient. The Δmag value is obtained by taking the median of the highest contrast values within the afore mentioned separation range. This median makes a good estimation of the bottom plateau value. Finally, Table 4 displays the upper mass limit for each object, i.e. that is the lowest mass we can safely exclude over the whole 30 to 500 mas range.

49 Ceti

49 Ceti is a main sequence A1V star identified to be a member of the 40 Myr old Argus association (Zuckerman & Song 2012). It is located at a distance of 59 ± 1 pc (van Leeuwen 2007). This disk is unusual because of its high density of gas, such as CO, compared to dust. It indicates a non-primordial gas presence likely to come from comet-like planetesimals collisions (Roberge et al. 2013).

Detection limits at 5σ on 49 Ceti give at least a contrast of 5×10^{-3} beyond 50 mas, up to 2×10^{-3} at 95 mas separation (Δmag of 5.8 and 8 respectively).

AU Microscopii

AU Mic is a young 0.3 $M_{\odot}$ M dwarf (Plavchan et al. 2009). Its age is estimated to be 8–20 Myr, and its Hipparcos distance is 9.9 pc (Perryman et al. 1997). It belongs to the β Pictoris moving group. It features a debris disk seen nearly edge-on (Kalas et al. 2004).

The youth and proximity of AU Mic are really favorable conditions to look for a low-mass detection domain. Recently, fast moving ripples in the disk have been observed. The ripples can be interpreted has signposts of significant planetary formation activity (Boccaletti et al. 2015).

Detection limits at 5σ on AU Microscopii give at least a contrast of $2.5{\times}10^{-3}$ beyond 50 mas, up to $9.5{\times}10^{-4}$ around 220 mas (Δmag of 6.5 and 7.6 respectively).

Beta Pictoris

β Pictoris is an A6V star located at 19.3 pc (van Leeuwen 2007). It belongs to the eponymous moving group, that was assumed to be 12^{+8}_{-4} Myr old (Zuckerman et al. 2001). Recently, a more precise – and possibly more accurate – measurement of the lithium depletion boundary gave an age for the moving group of 21 ± 4 Myr (Binks & Jeffries 2014). The β Pictoris system was the first optically resolved disk (Smith & Terrile 1984) and possesses a directly imaged exoplanet with one of the closest estimated semi-major axis to date: β Pictoris b (Lagrange et al. 2010; Chauvin et al. 2012; Bonnefoy et al. 2014).

Considering the position of β Pictoris b, it is within the field of view of NaCo/SAM. Despite the absence of detection through closure phases, we can constrain an upper L' band contrast ratio – and mass limit – at that position. Thanks to the orbital characterization by Chauvin et al. (2012) and concomitant observations by Nielsen et al. (2014), we estimated β Pictoris b to be situated at position $\Delta\alpha = -0.238''$ and $\Delta\delta = -0.385''$ during the observations reported here. The position is displayed in Fig. 3. The corresponding mass in terms of limits of detection (LOD) is $m_{\rm LOD} = 30\ M_{\rm Jup}$ (Δmag = 6.2). This value is consistent with the non-detection of β Pic b which has an estimated mass of $10^{+3}_{-2}\ M_{\rm Jup}$ (Bonnefoy et al. 2014).

Detection limits at 5σ on β Pictoris b give a fairly constant contrast between 5×10^{-3} and 2.5×10^{-3} (Δmag of 5.8 and 6.5 respectively) beyond 70 mas.

Eta Telescopii

Eta Telescopii (HR 7329A) is an A0V star. It is located at 47.7 pc according to Wyatt et al. (2007) and is also a member of the β Pictoris moving group. It possesses a companion HR 7329B at a 4 arcsec separation, out of the field of view of NaCO/SAM instrument. η Tel has also a more distant stellar companion HD 181327 at a 7 arcmin separation.

Detection limits at 5σ on η Telescopii give, at least, a contrast varying between 4×10^{-3} and 1.8×10^{-3} (Δmag of 6 and 6.9 respectively) beyond 50 mas.

Fomalhaut

Fomalhaut is a A3V/A4V star located at only 7.7 pc from the Sun. Fomalhaut's dust disk was initially discovered because of its infrared excess in IRAS observations by Aumann (1985). Fomalhaut's dust belt was optically resolved by Kalas et al. (2005) using the advanced camera for surveys (ACS) on the *Hubble* space telescope (HST). The first optical image of an extra-solar planet around this system was obtained with the HST later on by Kalas et al. (2008). Contrary to AU Mic or β Pic, Fomalhaut's disk is not seen edge on, so it provides a better insight into the innermost region.

The very good seeing during the observation allowed to reach a 5σ contrast ratio limit of $4.4{\times}10^{-4}$ within 50 to 200 mas. However the relatively old age of Fomalhaut (440 Myr, Mamajek 2012) explains the high-mass limit we obtain, since evolutionary models predict a decrease in luminosity with age.

A compilation of measurements from literature was done by Kenworthy et al. (2013). It gathered coronographic data from *Spitzer* (4.5 μm) and VLT/NaCo (4.05 μm) as well as VLTI/PIONIER interferometric data. Those measurements cover a large range of angular separation (1 to 2000 mas), nevertheless a gap in coverage remained from 100 to 200 mas. Kenworthy et al. pointed out in their Discussion section that SAM techniques would bridge the gap. With our present measurements we indeed fill that gap. We can also highlight that we provide noticeably lower mass limit than VLTI/PIONIER did over 50 to 100 mas.

Detection limits at 5σ on Fomalhaut give at least a contrast varying between 1.9×10^{-3} and 1.2×10^{-3} (Δmag of 6 and 6.9 respectively) beyond 50 mas.

g Lupi

g Lupi (also know as HD139664) is a F5V main sequence star located at 17.5 pc (van Leeuwen 2007). It is a member of the Hercules-Lyra association (López-Santiago et al. 2006). Dust scattered light was first observed using a coronagraph on the HST (Kalas et al. 2006). It revealed a disk structure seen nearly edge-on extending out to 109 AU.

The age of g Lupi is not well constrained but various age indicators suggest that the system is 300 million years old. The uncertainties concerning the age of 300^{+700}_{-200} Myr imply a respective variation of $\pm 25\ M_{\rm Jup}$ in our upper mass limits.

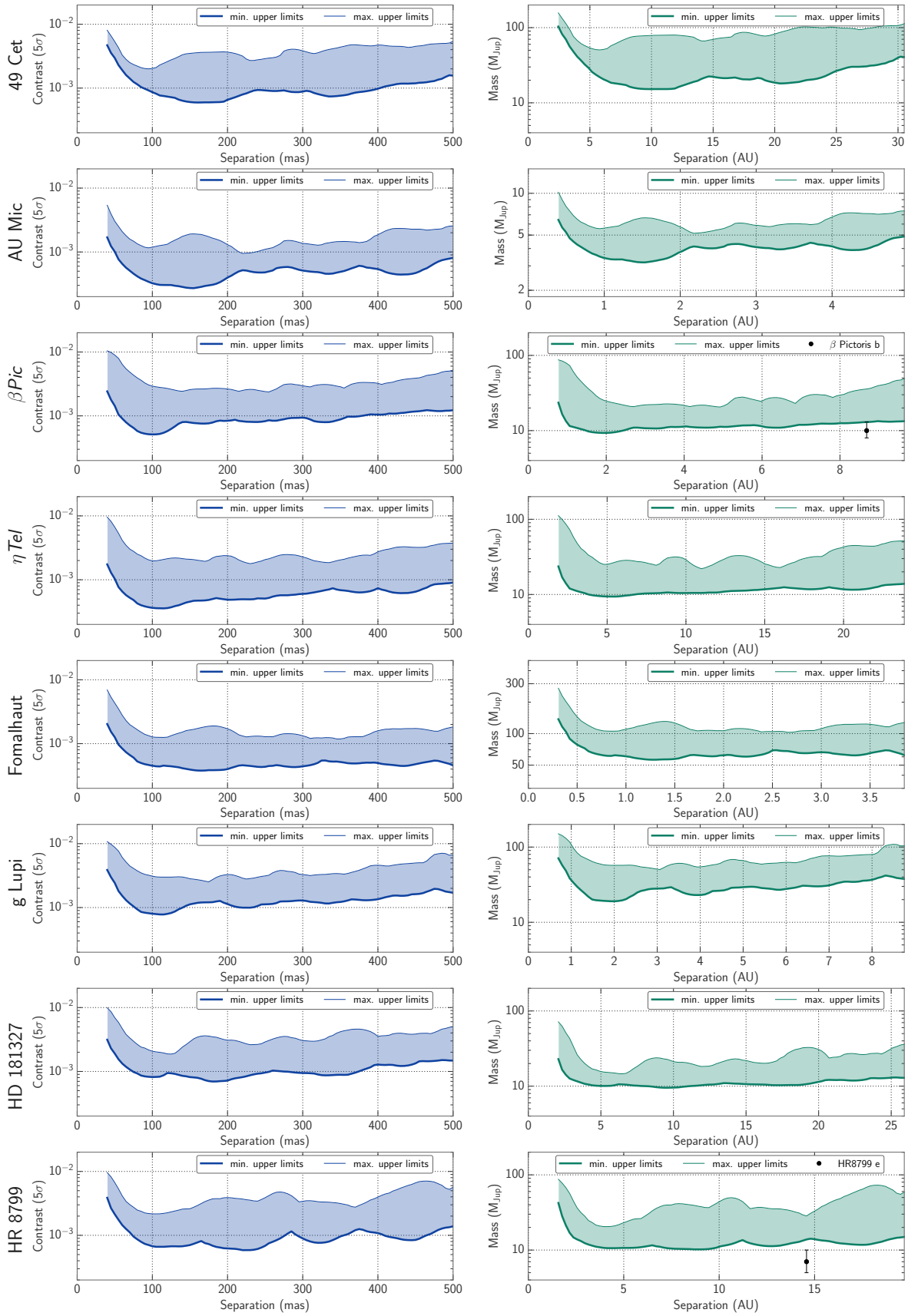

Fig. 4. Radial distribution of the detection limits. On the *left*, blue graphs display contrast as a function of the angular distance in milliarcseconds, this expresses the performance of the detection. On the *right*, green graphs display estimated mass detection limits (according to the BT-Settl model) as a function of separation in AU. In order to keep track of the azimuthal variation, the lower thick line represents the minimum value found at a given radial distance *r*, while upper thin line is the maximum value. Black dots represent companion within the known planetary systems.

Table 3. Highest-contrast capabilities of SAM mode on NaCo.

Object	Δmag (mag)	contrast ratio (5σ)	Mass (M_{jup})	Distance (AU)
49 Cet	7.86	7.2×10^{-4}	17.6	8–12
AU Mic	8.72	3.2×10^{-4}	3.4	1–2
β Pic	7.79	7.6×10^{-4}	10.7	1–3
η Tel	8.32	4.7×10^{-4}	10.3	4–7
Fomalhaut	8.39	4.4×10^{-4}	61.1	1–2
g Lup	7.44	1.1×10^{-3}	24.5	1–3
HD 181327	7.71	8.2×10^{-4}	9.9	5–10
HR 8799	7.92	6.8×10^{-4}	10.7	4–8

Table 4. Upper mass limits: lowest mass we can safely exclude within 30 to 500 mas separation.

Object	Δmag (mag)	contrast ratio (5σ)	Mass (M_{jup})
49 Cet	5.24	8.0×10^{-3}	156.9
AU Mic	5.67	5.4×10^{-3}	10.1
β Pic	4.96	1.0×10^{-2}	87.9
η Tel	5.05	9.6×10^{-3}	114.1
Fomalhaut	5.40	6.9×10^{-3}	273.3
g Lup	4.92	1.1×10^{-2}	154.2
HD 181327	5.01	9.9×10^{-3}	73.2
HR 8799	5.04	9.6×10^{-3}	87.3

Detection limits at 5σ on g Lupi give at least a contrast of 6×10^{-3} beyond 50 mas, up to 2.5×10^{-3} at 175 mas (Δmag of 5.5 and 6.5 respectively).

HD 181327

HD 181327 is an F5V/F6V star located at 39.4 pc and assumed to be a member of the β Pictoris moving group (Zuckerman & Song 2004). It was identified as a debris disk candidate based on the detection of far-IR luminosity excess (Mannings & Barlow 1998). PSF-subtracted coronagraphic observations on HST data revealed a debris ring at 86 AU radius from the star Schneider et al. (2006), Herschel/PACS observations showed the presence of a Kuiper's belt-like structures populated of icy planetesimals Chen et al. (2008).

Detection limits at 5σ on HD 181327 give at least a contrast of 5×10^{-3} beyond 50 mas, up to 1.8×10^{-3} at 125 mas (Δmag of 5.8 and 6.8 respectively).

HR 8799

HR 8799 is a member of the ~30 Myr old Columba association (Marois et al. 2010; Baines et al. 2012). The star is an F0V star located at 39.4 pc from Earth (van Leeuwen 2007).

Our detection limits are in good agreement with those derived by Hinkley et al. (2011) using the same technique at Keck telescope. This highlights the robustness of non-redundant masking techniques. In the same way we have done on β Pictoris, we used Marois et al. (2010) to estimate the HR 8799 companion *e* position. At the time of observation, we expect it to be at the position $\Delta\alpha = -0.353''$ and $\Delta\delta = -0.108''$. At these coordinates we find a corresponding upper mass boundary $m_{LOD} = 19\ M_{Jup}$ (Δmag = 7.4).

Detection limits at 5σ on HR 8799 give at least a contrast of 7×10^{-3} beyond 50 mas, up to 2.2×10^{-3} (Δmag of 5.4 and 6.7 respectively).

4. Conclusions

The SAM technique allows for probing the very nearby environment of the star that is usually inaccessible to conventional direct imaging image processing. It combines high angular resolution and high-contrast detection which are key elements in the study of planetary system formation.

While no companion has been detected in our SAM observational data, we have been able to set upper mass limits on potential companions presence within the 30 to 500 mas range. This was done for each one of the eight debris disks reported in this study.

Especially, this data provides clarification on the presence of close companions that may have ejected known ones on more distant orbits from the star. β Pic has an inclined orbit relatively to the main disk, this can hardly be explained otherwise than by a past dynamical interaction. HR 8799 planets cannot have formed in-situ by a core accretion process as described by Pollack et al. (1996) and may have been ejected by bodies closer to the star. η Tel B is a brown dwarf with a large separation which appears to be situated beyond the outer edge of the debris disk of its parent star, but that might have formed in the initial disk by gravitational instability (Cameron 1978). Fomalhaut b possesses a very eccentric orbit, that might also be explained by ejection from a previous orbit. For each object, these observations allow us to exclude the presence of a range of massive bodies that might have modified the initial orbit of known companions.

The SAM technique associated with star hopping is particularly efficient when the correction of the wavefront is good, which is the case with NACO in L'. The SAM mode to be commissioned on SPHERE at the VLT will make it possible to do even better in $Y-J-H$ and K bands in the near future. This technique is recognized to be highly competitive in the brown dwarf desert exploration, and plays an important part in the study of the role of multiplicity in low-mass stellar formation and migration mechanisms.

Acknowledgements. L. Gauchet would like to thank the referee Markus Feldt for his thorough review of the paper and his constructive comments, which significantly improved the quality of the publication. This work was supported by the French National Agency for Research (ANR-13-JS05-0005-01) and the European Research Council (ERC-STG-639248). A.-M. Lagrange acknowledges the support from the ANR blanche GIPSE (ANR-14-CE33-0018) and the Labex OSUG.

References

Allard, F., Homeier, D., & Freytag, B. 2012, Phil. Trans. R. Soc. Lond. A: Math. Phys. Eng. Sci., 370, 2765
Aumann, H. H. 1985, PASP, 97, 885
Aumann, H. H., Beichman, C. A., Gillett, F. C., et al. 1984, ApJ, 278, L23
Baines, E. K., White, R. J., Huber, D., et al. 2012, ApJ, 761, 57
Baldwin, J. E., Haniff, C. A., Mackay, C. D., & Warner, P. J. 1986, Nature, 320, 595
Baraffe, I., Chabrier, G., Allard, F., & Hauschildt, P. 1997, A&A, 327, 1054
Baraffe, I., Chabrier, G., Allard, F., & Hauschildt, P. H. 1998, A&A, 337, 403
Baraffe, I., Chabrier, G., Barman, T. S., Allard, F., & Hauschildt, P. H. 2003, A&A, 402, 701
Binks, A. S., & Jeffries, R. D. 2014, MNRAS, 438, L11
Boccaletti, A., Thalmann, C., Lagrange, A., et al. 2015, Nature, 526, 230
Bonnefoy, M., Boccaletti, A., Lagrange, A., et al. 2013, A&A, 555, A107
Bonnefoy, M., Currie, T., Marleau, G., et al. 2014, A&A, 562, A111
Cameron, A. G. W. 1978, The Moon and the Planets, 18, 5

Chauvin, G., Lagrange, A., Beust, H., et al. 2012, A&A, 542, A41
Chen, C. H., Fitzgerald, M. P., & Smith, P. S. 2008, ApJ, 689, 539
Cutri, R. M., Skrutskie, M. F., van Dyk, S., et al. 2003, VizieR Online Data Catalog: II/246
Ducati, J. R. 2002, VizieR Online Data Catalog: II/237
Gray, R. O., & Corbally, C. J. 2014, AJ, 147, 80
Gray, R. O., Corbally, C. J., Garrison, R. F., et al. 2006, AJ, 132, 161
Greenbaum, A. Z., Pueyo, L., Sivaramakrishnan, A., & Lacour, S. 2015, ApJ, 798, 68
Haniff, C. A., Mackay, C. D., Titterington, D. J., et al. 1987, Nature, 328, 694
Hinkley, S., Carpenter, J. M., Ireland, M. J., & Kraus, A. L. 2011, ApJ, 730, L21
Holmberg, J., Nordström, B., & Andersen, J. 2009, A&A, 501, 941
Kalas, P., Liu, M. C., & Matthews, B. C. 2004, Science, 303, 1990
Kalas, P., Graham, J. R., & Clampin, M. 2005, Nature, 435, 1067
Kalas, P., Graham, J. R., Clampin, M. C., & Fitzgerald, M. P. 2006, ApJ, 637, L57
Kalas, P., Graham, J. R., Chiang, E., et al. 2008, Science, 322, 1345
Kennedy, G. M., & Kenyon, S. J. 2008, ApJ, 682, 1264
Kenworthy, M. A., Meshkat, T., Quanz, S. P., et al. 2013, ApJ, 764, 7
Lacour, S., Tuthill, P., Amico, P., et al. 2011, A&A, 532, A72
Lagrange, A., Bonnefoy, M., Chauvin, G., et al. 2010, Science, 329, 57
Lohmann, A. W., Weigelt, G., & Wirnitzer, B. 1983, Appl. Opt., 22, 4028
López-Santiago, J., Montes, D., Crespo-Chacón, I., & Fernández-Figueroa, M. J. 2006, ApJ, 643, 1160
Mamajek, E. E. 2012, ApJ, 754, L20
Mannings, V., & Barlow, M. J. 1998, ApJ, 497, 330
Marois, C., Zuckerman, B., Konopacky, Q. M., Macintosh, B., & Barman, T. 2010, Nature, 468, 1080
Nielsen, E. L., Liu, M. C., Wahhaj, Z., et al. 2014, ApJ, 794, 158
Perryman, M. A. C., Lindegren, L., Kovalevsky, J., et al. 1997, A&A, 323, L49
Plavchan, P., Werner, M. W., Chen, C. H., et al. 2009, ApJ, 698, 1068
Pollack, J. B., Hubickyj, O., Bodenheimer, P., et al. 1996, Icarus, 124, 62
Roberge, A., Kamp, I., Montesinos, B., et al. 2013, ApJ, 771, 69
Schneider, G., Silverstone, M. D., Hines, D. C., et al. 2006, ApJ, 650, 414
Smith, B. A., & Terrile, R. J. 1984, Science, 226, 1421
Spiegel, D. S., & Burrows, A. 2012, ApJ, 745, 174
Stauffer, J., Tanner, A. M., Bryden, G., et al. 2010, PASP, 122, 885
Tokunaga, A. T. 2000, in Allen's astrophysical quantities, 4th edn., ed. A. N. Cox, 143
Torres, C. A. O., Quast, G. R., da Silva, L., et al. 2006, A&A, 460, 695
Tuthill, P., Monnier, J., Danchi, W., Wishnow, E., & Haniff, C. 2000, PASA, 112, 555
van Leeuwen, F. 2007, A&A, 474, 653
Weigelt, G. P. 1977, Opt. Comm., 21, 55
Wyatt, M. C., Smith, R., Su, K. Y. L., et al. 2007, ApJ, 663, 365
Zuckerman, B., & Song, I. 2004, ApJ, 603, 738
Zuckerman, B., & Song, I. 2012, ApJ, 758, 77
Zuckerman, B., Song, I., Bessell, M. S., & Webb, R. A. 2001, ApJ, 562, L87